SCIENTIFIC PAPER

Suppressing Pre-hydrolysis in TiO_2 Manufacturing: Design Optimization of an Indirect Heating Hydrolysis System

Junhee Han[1], Hyojung Kim[2], Dohyung Lee*[3]

[1] Department of Mechanical engineering, Hanyang University, Seoul, KOREA

[2] Ackerton Partners, 41, Cheonggyecheon-ro, Jongno-gu, Seoul, KOREA

[3] Department of Mechanical engineering, Hanyang University, Ansan, Gyeonggi-do, KOREA

https://doi.org/10.2298/CICEQ230731031H

Received 31.7.2023.

Revised 1.8.2024.

Accepted 26.8.2024.

* Address all correspondence to: Dohyung Lee, Tel.: +82 31-400-5289, E-mail: Dohyung@hanyang.ac.kr

Abstract

The particle size of TiO_2 is critically influenced by the operation of the hydrolysis process. Failure to achieve uniform particle size during hydrolysis can have significant repercussions on subsequent processes, such as washing, reduction and bleaching procedures, ultimately leading to the production of unusable final products. The primary goal of this study is to suppress pre-hydrolysis, which is a factor that impedes the formation of uniform particles during the hydrolysis procedure. To overcome this issue, the researchers designed an indirect heating system to mitigate the pre-hydrolysis phenomenon. For designing indirect heating system, multiphase Computational Fluid Dynamics (CFD) simulations were performed. The proposed optimized design was then implemented and tested in the actual field. The success of the field test was evaluated through settling value tests conducted on the hydrolyzed solution, and the uniformity of particle size was analyzed using Transmission Electron Microscopy (TEM) images, Scanning Electron Microscope (SEM) and Microtrac. The findings of this study demonstrate the effective application of the developed multiphase CFD simulation in enhancing the hydrolysis process for the production of anatase titanium dioxide particles. This successful integration demonstrates the application of mechanical engineering techniques in the fields of chemical engineering.

KEY WORDS: Multiphase, Conjugate CFD simulation, precipitation, particle size distribution, TiO_2 manufacturing, indirect heating hydrolysis.

Highlights:

- Indirect heating system was developed for inhibiting TiO2 pre-hydrolysis.
- Multiphase heat transfer CFD simulation with immersed solid method was conducted
- The optimized indirect heating system has been stably operated in the real field.
- Uniformity of TiO2 particles was confirmed by the Settling Value test and TEM analysis

Introduction

Titanium dioxide is a widely used white pigment in industries such as coatings, paints, paper, plastic, rubber, ceramics, and textiles. There are two main structures of titanium dioxide particles: rutile and anatase, depending on the production method [1,2]. This paper will specifically focus on the sulfate process, which involves the decomposition of titanium-containing raw materials through sulfuric acid and subsequent hydrolysis of titanium sulfate [3]. The chemical reactions integral to the sulfate process are illustrated in Eq.(1) below.

$$\begin{gathered} FeTiO_3 + 2H_2SO_4 \rightarrow FeSO_4 + TiOSO_4 + 2H_2O \\ TiOSO_4 + (n+1)H_2O \rightarrow TiO_2 \bullet nH_2O + H_2SO_4 \\ TiO_2 \bullet H_2O \rightarrow TiO_2 + nH_2O \end{gathered} \quad (1)$$

To achieve high-quality white pigment production, precise and stable control of the hydrolysis process is essential. Many TiO_2 manufacturing industries have undertaken efforts to optimize this process [4-8]. The typical hydrolysis procedure for TiO_2 manufacturing involves introducing high-temperature steam into a $TiOSO_4$ solution using bottom-mounted steam nozzles. After reaching a specific temperature (96℃), external seeds are added to initiate hydrolysis [9-11]. However, the initial heating phase can lead to temperatures exceeding 110℃ at the nozzle location, potentially causing pre-hydrolysis before seed introduction [12,13]. This pre-hydrolysis leads to the formation of particles smaller than 100 nm, which can clog filter cloth pores during washing. This phenomenon acts as a bottleneck that directly impacts the overall manufacturing capacity [14,15]

The most effective approach to prevent pre-hydrolysis is to perform the first heating step using water-free heat source [16]. Subsequently, the second and third heating steps, where seeds are present, should utilize conventional steam direct heating appropriately. To achieve this, a preheating tank with an indirect heating system using a heating coil is proposed for first heating procedure and it should be positioned prior to the existing hydrolysis tank.

The design of the indirect preheating tank requires multiphase CFD simulation to handle the two phases present: The $TiOSO_4$ solution filled inside the tank and the steam flowing into the heating coil. The simulation will help in identifying an appropriate shape of

heating coil, which can uniformly heat the solution up to 96℃ within 20 minutes.

However, conducting multiphase CFD simulations presents challenges in terms of computing power and time, especially when compared to single-phase simulations. This complexity arises from considering multiple working fluids and boundary interfaces. In cases involving rotating fluid machinery within multiphase CFD simulations, the mesh must be regenerated at each time step to account for the interface between the rotating and stationary regions. This re-meshing process demands a considerable amount of additional computing power

Therefore, many researchers have developed CFD method to reduce computing time, such as the moving reference frame (MRF) [17,18], sliding mesh (SM) [19-21], overlapping grid [22,23] and so on. However, these methods often sacrifice accuracy for computational efficiency and are mainly used for steady-state simulations. In this study, since the time-dependent temperature distribution and heat transfer are crucial, we aim to explore the Immersed Solid Mesh (ISM) technique along with these methods to reduce computational time while preserving accuracy [24-28] In traditional applications, the Immersed Solid Method (ISM) has primarily been utilized for tracking the trajectories of solid particles within a Discrete Element Method (DEM), where considerations of mass transfer or heat transfer are not included.

However, this study aims to utilize the Immersed Solid Method (ISM) to conduct a multiphase simulation, which includes heat transfer between a fluid and gas through heating coil solid body. By employing ISM, the computational domain can be extended to virtually model the solid structures surrounding the fluid, leading to enhanced accuracy in the analysis and reducing the necessity for frequent mesh generation and updates. By analyzing the heat distribution inside the tank and on the surface of the heating coil, this study aims to optimize the design of the heating coil for an indirect heating system.

MULTI-PHASE CFD SIMULATION

Governing Equation

The Navier-Stokes equation serves as the principal governing equation for general single-phase Computational Fluid Dynamics (CFD) applications, represented as Eq.(2).

$$\rho g_x - \frac{\rho p}{\rho x} + \frac{\partial}{\partial x}\left(2\mu\frac{\partial u}{\partial x} - \frac{2}{3}\mu\nabla\cdot\vec{V}\right) + \frac{\partial}{\partial y}\left[\mu\left(\frac{\partial u}{\partial y} + \frac{\partial v}{\partial x}\right)\right] + \frac{\partial}{\partial z}\left[\mu\left(\frac{\partial w}{\partial x} + \frac{\partial u}{\partial z}\right)\right] = \rho\frac{\partial u}{\partial t} + \rho(\vec{V}\cdot\nabla)u \qquad (2)$$

In a typical multiphase CFD solver, when two different phases of fluids come into contact, force and mass exchange occur, leading to the formulation of equations like Eq.(3) and Eq.(4).

$$\text{Continuity}: \frac{\partial(\alpha_q\rho_q)}{\partial t} + \nabla\cdot\left(\alpha_q\rho_q u_q\right) = \sum_{p=1}^{n}\dot{m}_{pq} \qquad (3)$$

$$\text{Energy}: \frac{\partial(\rho U)}{\partial t} - \frac{\partial\rho}{\partial t} + \nabla\cdot(\rho U h_{tot}) = \nabla\cdot(\kappa\,\nabla T) + \nabla\cdot(U\,\nabla\tau) + S_M \qquad (4)$$

The meaning of α_q is the Volume fraction of q^{th} phase, and the momentum equation of q^{th} phase can be written as the following Eq.(5)

$$\frac{\partial\left(\alpha_q\rho_q u_q\right)}{\partial t} + \nabla\cdot\left(\alpha_q\rho_q u_q\right) = \\ = -\alpha_q\nabla p + \alpha_q\rho_q g + \nabla\cdot\tau_q + \sum_{p=1}^{n}\left(R_{pq} + \dot{m}_{pq}u_q\right) + \alpha_q\rho_q\left(F_q + F_{lift,q} + F_{vm,q}\right) \qquad (5)$$

Where R_{pq} is interphase forces exchange, and $\dot{m}_{pq}u_q$ is interphase mass exchange. However, in this study, the heating coil inhibits mass exchange between two different phases and only allows heat exchange between them. As a result, terms related to R_{pq}, $\dot{m}_{pq}u_q$ become zero during the calculation process, and only heat transfer through volume calculations of different phases is considered.

CFD procedure and results

Geometry and mesh generation

The tank present on the site has dimensions of 3.35m x 3.45m and features a 5° downward slope at the base to facilitate liquid drainage. Inside the tank, there are two-stage blades with a 45° pitch angle for smooth solution mixing, along with an indirect heating coil. The actual field geometry is illustrated in fig 1(a) and computational geometry is explained in

fig1(b).

Figure 1

Two different methods can be used for mesh generation: the conventional method of General Grid Interfacing (GGI), and a simpler method utilizing the Immersed Solid Method (ISM). These two types of mesh generations are explained in fig1 (c). When generating the mesh using the immersed solid mesh (ISM) method ~~with ANSYS CFX 18.2 mesh program~~, the total number of mesh elements was reduced by over 20% compared to using the GGI (General Grid Interface) method, while keeping the same growth rate and mesh setup values. Specifically, the GGI method resulted in an approximately 8.8 million mesh elements, whereas the ISM approach yielded a mesh with 5.9 million elements. Comparing the Immersed Solid Method (ISM) with the GGI method, the ISM technique led to a remarkable 25% reduction in computation time for a total simulation timestep of 20 minutes. The GGI method required 72 hours, while the ISM method completed the simulation in 54 hours. Additionally, when assessing the average temperature of $TiOSO_4$ solution, both methods exhibited a temperature deviation of less than 1 degree. Therefore, in this study, the Immersed Solid Method (ISM) approach was employed while maintaining the accuracy of CFD calculations. The temperature rise curves calculated using the GGI method and the immersed solid mesh are shown in Figure 1(d). The curves indicate that there is little difference in the temperature rise, with the GGI method requiring 59 hours of computing time for a 20-minute real-time step, while the immersed solid mesh required 41 hours. However, due to the mesh not being fine enough, the accurate capture of eddy movements near the blunt body was not achieved, resulting in slight differences in the temperature contour.

Therefore, the simulation using the immersed solid mesh is a suitable method for scenarios like optimization processes where high accuracy is not essential, and many cases need to be computed in a short amount of time, similar to the DOE (Design of Experiments) method.

Boundary condition

The tank is filled with $TiOSO_4$ solution and high-pressure steam at 5 bar and 185℃ is supplied through the heating coil. The steam outlet is set as an opening condition because it

is not subjected to any external pressure and is open to atmospheric pressure. Table 1 describes the properties of the working fluid.

Table 1

The heat transfer process involves two distinct heat interfaces. The first interface encompasses the inner surface of the pipe through which steam is introduced, coming into direct contact with the steel material. The second heat interface is formed at the contact surface between the steel material and the $TiOSO_4$ solution. This simulation specifically considers heat transfer exclusively across these interfaces. For the steel material, 10mm thickness 100A of 316L stainless steel property was used for heat conductivity, thermal expansion coefficient. The Agitator, using the Immersed Solid Method, rotates clockwise at 35 rpm, while the wall is subjected to a no-slip boundary wall condition.

Simulation results

To initiate the seed injection process, The $TiOSO_4$ solution in the indirect heating tank should be heated up to target temperature of 96°C in 20 minutes. Firstly, performance evaluation of single heating coil was carried out. The height of the coil was limited to 2000mm from the bottom, taking into account the height of the liquid and the agitator blade. Figure. 2 represents the temperature contour on the surface of the single heating coil and streamline at side plane of tank. It demonstrates that the temperature distribution on the heating coil surface varies according to the fluid flow.

Figure 2

This emphasizes the results of heat transfer between gas-solid-fluid, which fundamentally differs from conventional CFD simulations that involve setting a heat source on a typical wall surface. In addition, in the region where the agitator rotates, the fluid exhibits high turbulence kinetic energy, leading to vigorous heat exchange between the heating coil and the $TiOSO_4$ solution. As a result, the temperature on the surface of the heating coil facing the agitator appears to be lower compared to other areas.

Table 2

As shown in Table 2, even though heat exchange was vigorous, it was not possible to reach the desired target temperature within the limited height and time using a single heating coil. When rotating the coil 10 times, the gap between the heating coils becomes less than 10cm. Based on past experience and CFD simulation, the possibility of scale formation between the coils becomes very high in such cases. Therefore, the simulations were conducted excluding the results after 10 rotations.

It is necessary to install the double heating coils to increase heating efficiency. In the design range, the heating coil was installed from 6 to 9 rotations, the same as in a single stage, and the heat change was observed for up to 20 minutes.

Table 3

As can be seen from the Table 3 and Fig. 3, it is evident that there is a significant incr ease in temperature from the 6th rotation to the 8th rotation. However, from the 8th rotations, there is no more temperature rise.

The inner heating coil surface facing to the agitator exhibits a relatively lower heat distribution compared to other areas due to the presence of active heat transfer with the $\boldsymbol{TiOSO_4}$ solution. On the other hand, the outer heating coil positioned facing to the wall has limited heat transfer to the solution, resulting in a relatively higher surface temperature distribution. Furthermore, as the number of coil revolutions increases, it can be observed that the outer portion of the heating coil fails to transfer heat effectively and still maintains a very high surface temperature.

Figure 3

Figure 4 illustrates the temperature distribution of the side plane, turbulence eddy dissipation and the velocity in the v direction. In the case of 6-rotation, the $TiOSO_4$ solution flows smoothly between the heating coils, allowing for sufficient heat transfer. On the contrary, in the case of 9-rotation, the narrow spacing between the heating coils hinders the flow of the working fluid.

Figure 4

The simulation results of this study demonstrated that the heating of the $TiOSO_4$ solution to 96℃ within the targeted 20 minute is achieved by the utilization of an 8-rotation double heating coil.

Lab scale test and results.

The results of calculated by CFD were tested in a lab-scale pilot facility reduced to a 38:1 scale. The $TiOSO_4$ solution, heated without the addition of moisture, underwent hydrolysis, reduction, washing, calcination, and milling processes. The particle distribution was analyzed using SEM and microtrac techniques. Figure 5 shows the particle distribution as determined by SEM analysis and microtrac. Particles within the target specification of 300–400 nm account for 50.49% and 51.02% of the total, while particles within the nominal specification of 200–500 nm account for 84.88% and 85.25% of the total.

Comparatively, the direct heating system with moisture injection showed a distribution of less than 80% in the same experiment, indicating an improvement of over 5% with the indirect heating system. However, real field tests show a proportion exceeding 90%. The approximately 5% difference is attributed to the effects of boiling bubbles during heating, despite matching the Froude number to ensure experimental similarity. The presence of bubbles introduces various forces, such as virtual force, lift force, drag force, lubrication force, and turbulence dispersion force, which differ between a 5m diameter tank and a 20cm tank.

This discrepancy highlights an area for future research. Nonetheless, the consistent trend in particle distribution observed in the experiments confirms the effectiveness of the indirect heating method and its applicability to real field tests.

Figure 5.

Actual field test and results.

The 8-rotation double indirect heating coil with optimized agitator design, which demonstrated the most favorable heat diffusion based on the simulation results [8], was

installed at the site. Subsequently, the settling value was examined to assess the outcomes. ~~Left side of Fig. 4 illustrates the appearance of optimized heating coil in the indirect heating tank. As depicted in the right side of Fig.4, it is showing that pre-hydrolysis is effectively suppressed, resulting in a noticeably darker brown coloration of the solution.~~

~~Figure 4~~

~~In this study,~~ A settling value test, widely employed for assessing particle size uniformity, was conducted to determine whether the indirect heating system inhibits pre-hydrolysis. The settling value test involves diluting 114ml (190g/L TiO_2) of the hydrolyzed solution with 300ml of water. After cooling to 25 degrees, additional water is added to make up a 500ml solution. After 30 minutes, the suspension length is measured. A high settling value indicates a broader accumulation of smaller particles in the gaps between larger particles, resulting in a longer suspension length. On the contrary, a low settling value demonstrates that larger than 400nm TiO_2 particles are uniformly generated and there are significant presence of voids between particles. Figure 6 as shown below, presents the results of the settling value test, where the length of the clear portion in the supernatant is measured and recorded as the settling value.

To conduct the settling value test, a hydrolyzed solution is required. The solution used for the test is obtained by completing the hydrolysis process with indirect heating for the primary heating and steam direct heating for the secondary and tertiary heating stages. The hydrolyzed solution obtained without using an indirect heating system exhibited an average settling value of 65mm/30min. Moreover, there were instances where defective hydrolyzed solutions with a settling value of even 70mm/30min, rendering them unusable, were occasionally generated. On the other hand, with indirect heating, the settling values remained favorable, ranging from 55mm/39min to 45mm/30min.

Table 4

The bottom side of fig. 6 represents TEM (Transmission Electron Microscopy) images of the indirect heating process, zoomed in at ~~5000x and~~ 10000x magnifications. It can be observed that the particles in the size range of 0.1 micrometers significantly decreased compared to the single blade agitator and direct heating methods. However, it is important to

note that TEM images alone cannot provide a definitive judgment. TEM serves as supporting evidence, but for quantitative comparison and analysis, it is more appropriate to compare the settling values test.

Figure 6

Conclusion and discussion

In this study, an indirect heating system for the efficient hydrolysis of $TiOSO_4$ solution was designed and optimized using multiphase computational fluid dynamics (CFD) simulations. The developed CFD solver, capable of handling gas-solid-fluid heat transfer in a multi-phase environment. The optimized design of the indirect heating system was further validated through real field tests, demonstrating its ability to generate TiO_2 particles with a high level of uniformity.

The results indicate that the indirect heating system effectively prevents pre-hydrolysis, addressing one of the major challenges faced in the hydrolysis process. This achievement is supported by advanced characterization techniques such as settling value test~~ and,~~ Transmission Electron Microscopy (TEM), Scanning Electron Microscope (SEM) and Microtrac. These results are providing insights into the particle size distribution and settling behavior of the hydrolysis products. The completed hydrolyzed from the first-stage heating procedure, achieved through the designed indirect heating system, successfully yields uniform particle sizes. Furthermore, this has enabled the overall stable operation of the hydrolysis process.

Furthermore, the successful implementation of the immersed solid method in multiphase CFD has been demonstrated, particularly in the context of rotating machinery. This achievement highlights its broad potential applicability within various areas of the chemical engineering industry.

"**Acknowledgement**

This research was supported by COSMO Chemical Co., Ltd.

REFERENCES

[1] X. Xiong, Z. Wang, F. Wu, X. Li, H. Guo, Adv. Powder Technol. 24 (2013) 60-67. https://doi.org/10.1016/j.apt.2012.02.002.

[2] K.H. Cheung, M.B. Pabbruwe, W.F. Chen, Ceram. Int. 47 (2021) 1609-1624. https://doi.org/10.1016/j.ceramint.2020.08.277.

[3] B. Grzmil, D. Grela, B. Kic, Pol. J. Chem. Technol. 11 (2009) 15-21. https://doi.org/10.2478/v10026-009-0030-1.

[4] K.D. Kim, S.H. Kim, H. Taik, Colloids Surf., A 254 (2005) 99-105. https://doi.org/10.1016/j.colsurfa.2004.11.033.

[5] E.A. Moskalenko, A.A. Sadovnikov, A.E. Baranchikov, A.E. Goldt, V.V. Kozik, V.K. lvanov, Curr. Microwave Chem. 1 (2014) 81-86. https://doi.org/10.2174/2213335601666140404163607.

[6] M. Danish, S. Ambreen, A. Chauhan, A. Pandey, J. Saudi Chem. Soc. 19 (2015) 557-562. https://doi.org/10.1016/j.jscs.2015.05.010.

[7] Y. Bessekhouad, D. Robert, J.V. Weber, J. Photochem. Photobiol., A 157 (2003) 47-53. https://doi.org/10.1016/S1010-6030(03)00077-7.

[8] J.H. Han, H.J. Kim, D.H Lee, J. Enhanced Heat Transfer 30 (2023) 1-20. http://doi.org/10.1615/JEnhHeatTransf.2023047657.

[9] E.A. Barringer, H.K. Bowen, Am. Chem. Soc. 1 (1985) 420-428. https://doi.org/10.1021/la00064a005.

[10] S. Mahshid, M. Askari, M.S. Ghamsari, J. Mater. Process. Technol. 189 (2007) 296-300. https://doi.o rg/10.1016/j.jmatprotec.2007.01.040.

[11] Q. Zhang, L. Gao, J. Guo, J. Eur. Ceram. Soc. 20 (2000) 2153-2158. https://doi.org/10.1016/S0955-2219(00)00085-6

[12] N. Shijie, L. Debao, L. Yunshi, Y. Ping, J. Nanosci. Nanotechnol. 17 (2017) 3430-3434. https://doi.org/10.1166/jnn.2017.12808

[13] D.C.M. Dutoit, M. Schneider, R. Hutter, A. Baiker, J. Catal. 161 (1996) 651-658.

https://doi.org/10.1006/jcat.1996.0227.

[14] U. Gesenhues, Chem. Eng. Technol. 26 (2003) 25-33. https://doi.org/10.1002/ceat.200390001.

[15] J. Olabarrieta, O. Monzon, Y. Belaustegui, J. Inaki, S. Zorita, Sci. Total Environ. 618 (2018) 551-560. https://doi.org/10.1016/j.scitotenv.2017.11.003.

[16] I. Plazl, S. Leskovsek, T. Koloini, Chem. Eng J. 59 (1995) 253-257. https://doi.org/10.1016/0923-0467(94)02953-9

[17] J.B. Joshi, N.K. Nere, C.V. Rane, B.N. Murthy, C.S. Mathpati, A.W. Patwardhan, V.V Ranade, Can. J. Chem. Eng. 89 (2011) 754-816. https://doi.org/10.1002/cjce.20446.

[18] H. Patil, A.K. Patel, H.J. Pant, A.V. Vinod, Hydraul. Eng. 27 (2021) 200-209. https://doi.org/10.1080/09715010.2018.1535921

[19] F. Chen, W. Zhong, D. Wan, Ocean. Eng. 257 (2022) 1-13. https://doi.org/10.1016/j.oceaneng.2022.111525.

[20] R. Steijl, G. Barakos, Int. J. Numer. Methods Fluids 58 (2008) 527-549. https://doi.org/10.1002/fld.1757.

[21] J. Mcnaughton, I. Afgan, D.D. Apsley, Int. J. Numer. Methods Fluids 74 (2013) 250-269. https://doi.org/10.1002/fld.3849.

[22] G. Desquesnes, M. Terracol, E. Manoha, P. Sagaut, J. Comput. Phys. 220 (2006) 355-382. https://doi.org/10.1016/j.jcp.2006.05.019.

[23] H. Orihara, H. Miyata, J. Mar. Sci. 8 (2003) 47-60. https://doi.org/10.1007/s00773-003-0163-5.

[24] Y. Guo, C.Y. Wu, C. Thornton, AIChE J. 59 (2013) 1059-1087. https://doi.org/10.1002/aic.13900.

[25] P. Zhao, J. Xu, X. Liu, W. Ge, J. Wang, Phys. Fluids 32 (2020) 1-12. https://doi.org/10.1063/5.0023423.

[26] S.H. Saraei, B. Peters, Powder Technol. 426 (2023) 118-125. https://doi.org/10.1016/j.powtec.2023.118603

[27] J. Wang, H. Liu, D. Xu, Z. Chen, K. Ma, Build. Sci. 160 (2019) 106-122. https://doi.org/10.1016/j.buildenv.2019.106208.

[28] R. Mitkov, M. Pantusheva, V. Naserentin, P. Hristov, A. Logg, IFAC Proc. Ser. 55 (2022) 179-184. https://doi.org/10.1016/j.ifacol.2022.08.069.

Figure captions:

Figure 1. Geometry of indirect heating system

Figure 2. Temperature distribution on single heating coils surface

Figure 3. Temperature distribution on double heating coils surface and stream line of $TiOSO_4$ solution

Figure 4. Indirect heating coil installation and $TiOSO_4$ solution

Figure 5. Comparison of settling values between direct heating and indirect heating

Figure 6. TEM analysis of indirect heating system

Table 1. Property of $\boldsymbol{TiOSO_4}$ and wet steam

Identification	$\boldsymbol{TiOSO_4}$	**Wet steam**
m (Molar mass)	159.92 g/mol	18.01528 kg/kmol
ρ (Density)	1.5954 g/cm^3	2.669 kg/m^3
c (Specific heat capacity)	1070 J/kg.K	2.3289 kJ/kg.K
η (Dynamic viscosity)	0.001kg/ms	0.000014 kg/ms
κ (Thermal conductivity)	0.6W/m.K	0.003 W/m.K
Initial condition	1atm, 55℃	5bar, 185℃

Table 2. Average temperature of different single heating coils

Coil rotation (times)	Temperature of $TiOSO_4$ after 20min (℃)
6	77
7	80
8	83
9	84

Table 3. Average temperature of different double heating coils

Coil rotation (times)	Temperature of $TiOSO_4$ after 20min (℃)
6	92.375
7	96.337
8	101.415
9	101.7

Table 4. Settling values of indirect heating system

Case	Settling value (mm/30min)	Case	Settling value (mm/30min)
1	51	4	48
2	55	5	45
3	52	6	49

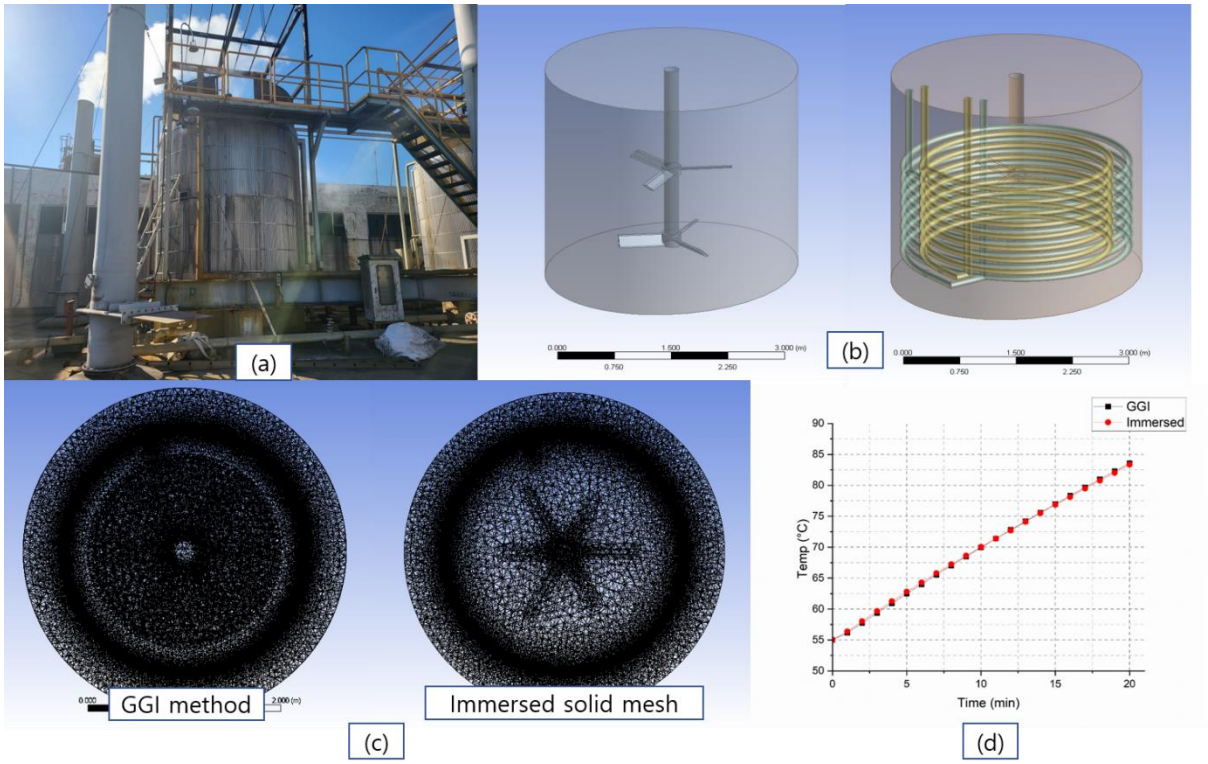
(a)
(b)
GGI method
Immersed solid mesh
(c)
GGI
Immersed
Temp (°C)
Time (min)
(d)

Figure 1

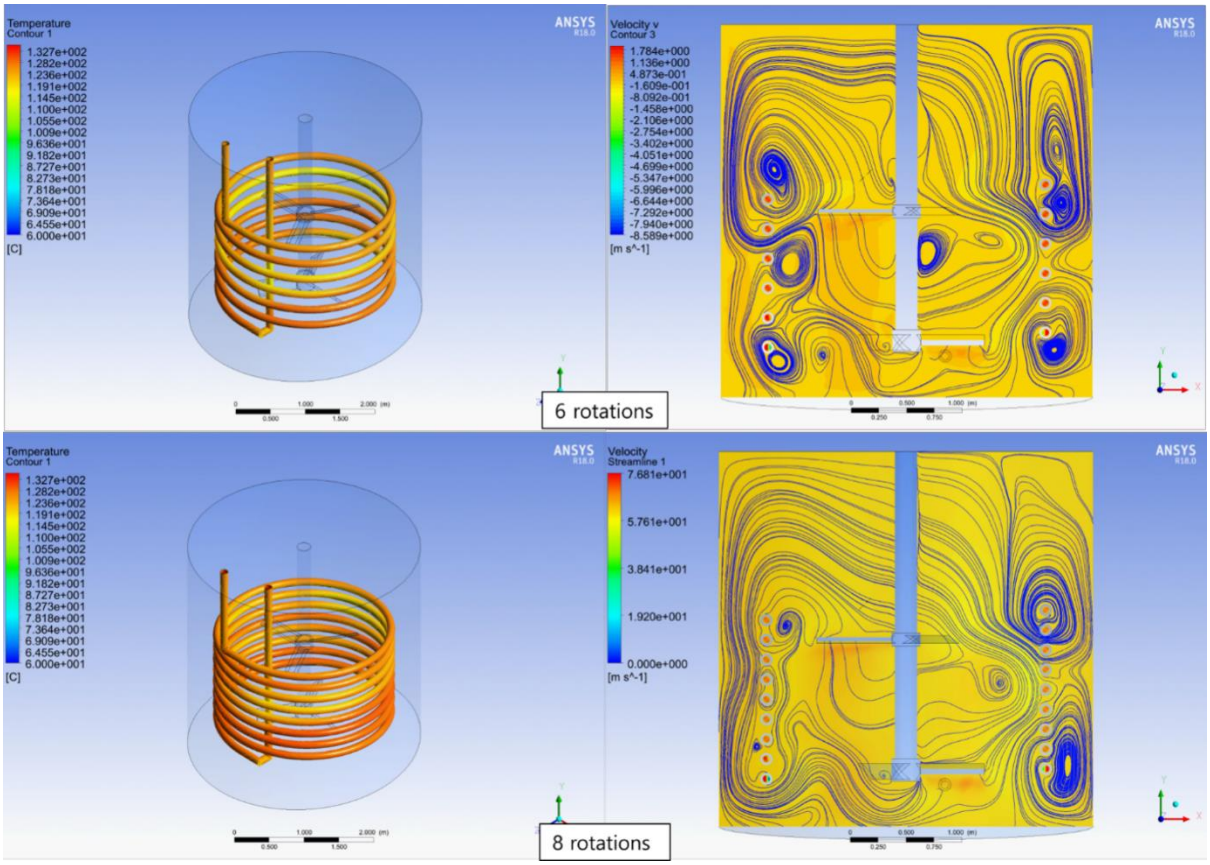
Temperature
Contour 1
1.327e+002
1.282e+002
1.236e+002
1.191e+002
1.145e+002
1.100e+002
1.055e+002
1.009e+002
9.636e+001
9.182e+001
8.727e+001
8.273e+001
7.818e+001
7.364e+001
6.909e+001
6.455e+001
6.000e+001
[C]
ANSYS
Velocity v
Contour 3
1.784e+000
1.136e+000
4.873e-001
-1.609e-001
-8.092e-001
-1.458e+000
-2.106e+000
-2.754e+000
-3.402e+000
-4.051e+000
-4.699e+000
-5.347e+000
-5.996e+000
-6.644e+000
-7.292e+000
-7.940e+000
-8.589e+000
[m s^-1]
6 rotations
Temperature
Contour 1
Velocity
Streamline 1
7.681e+001
5.761e+001
3.841e+001
1.920e+001
0.000e+000
8 rotations

Figure 2

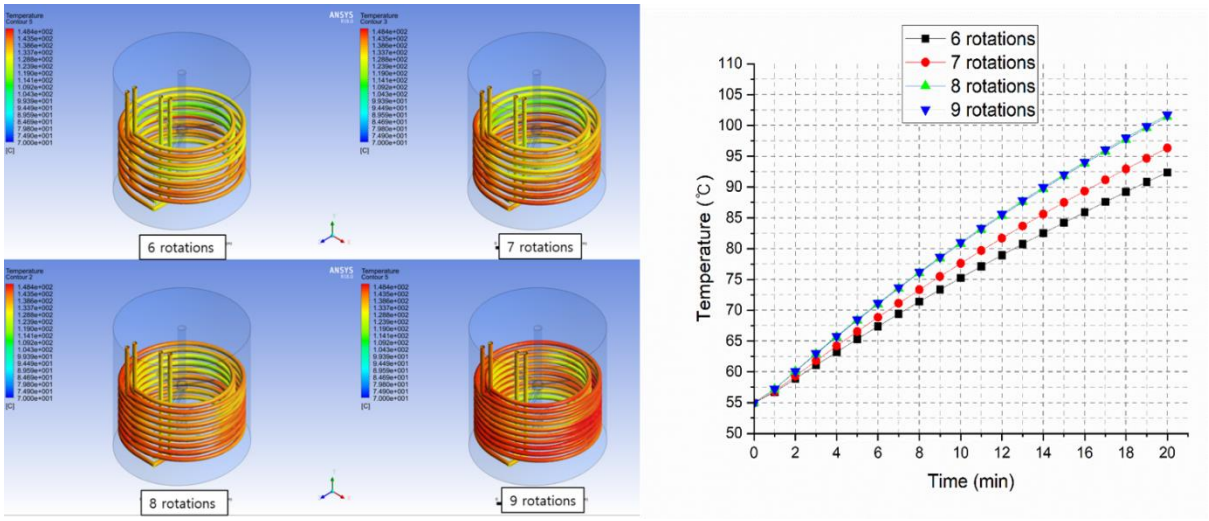
6 rotations
7 rotations
8 rotations
9 rotations
6 rotations
7 rotations
8 rotations
9 rotations
Temperature (℃)
Time (min)
110
105
100
95
90
85
80
75
70
65
60
55
50
0
2
4
6
8
10
12
14
16
18
20

Figure 3

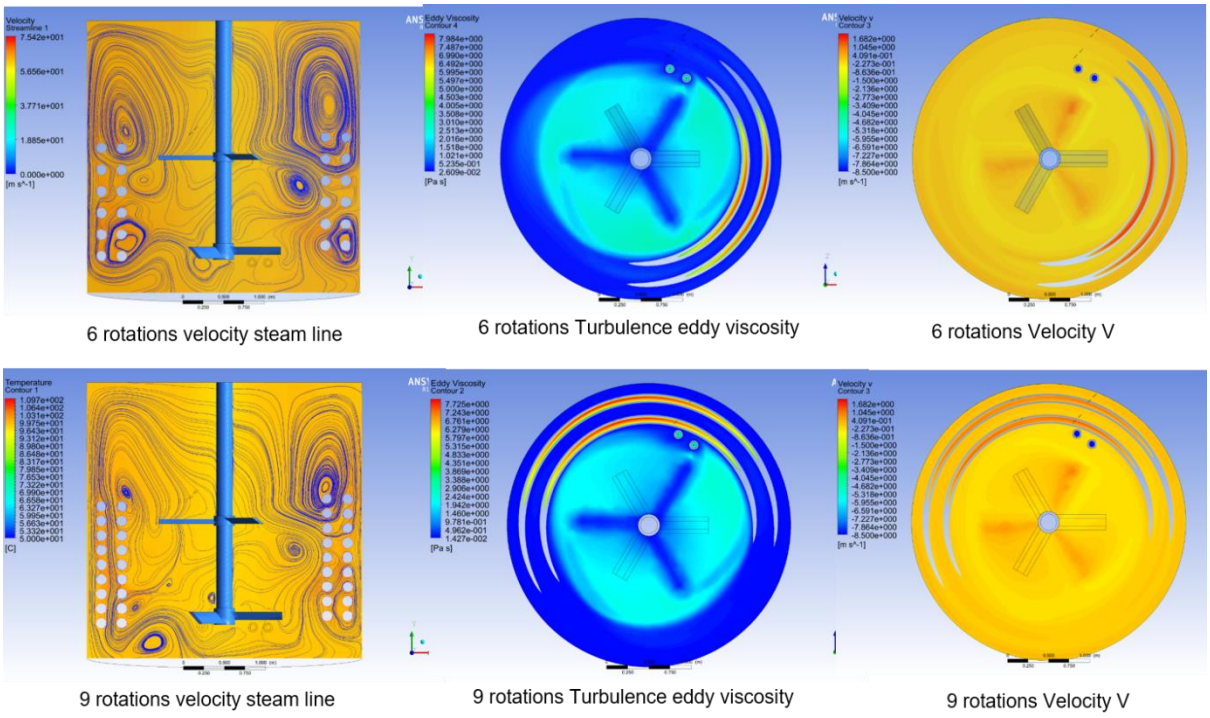
6 rotations velocity steam line
6 rotations Turbulence eddy viscosity
6 rotations Velocity V
9 rotations velocity steam line
9 rotations Turbulence eddy viscosity
9 rotations Velocity V

Figure 4

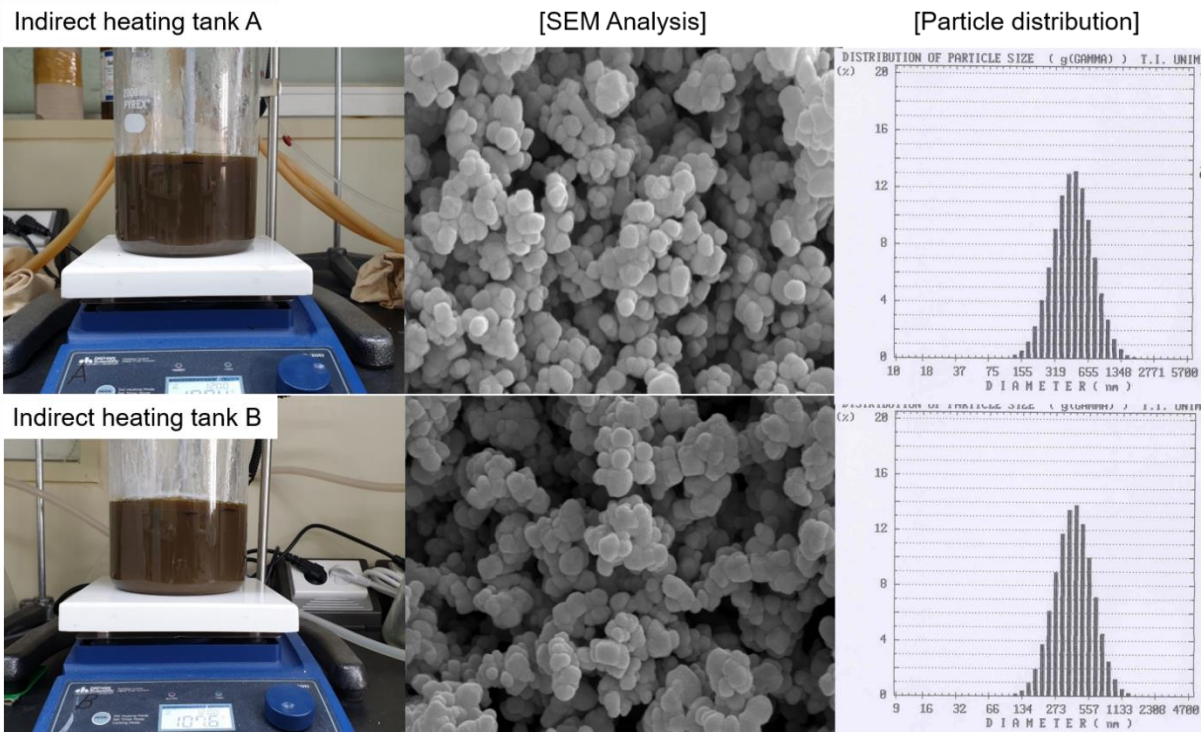
Indirect heating tank A
[SEM Analysis]
[Particle distribution]
DISTRIBUTION OF PARTICLE SIZE (g(GAMMA)) T.I. UNIM
(x) 20
16
12
8
4
0
18 18 37 75 155 319 655 1348 2771 5700
D I A M E T E R (nm)
Indirect heating tank B
(x) 20
16
12
8
4
0
9 16 32 66 134 273 557 1133 2388 4700
D I A M E T E R (nm)

Figure 5

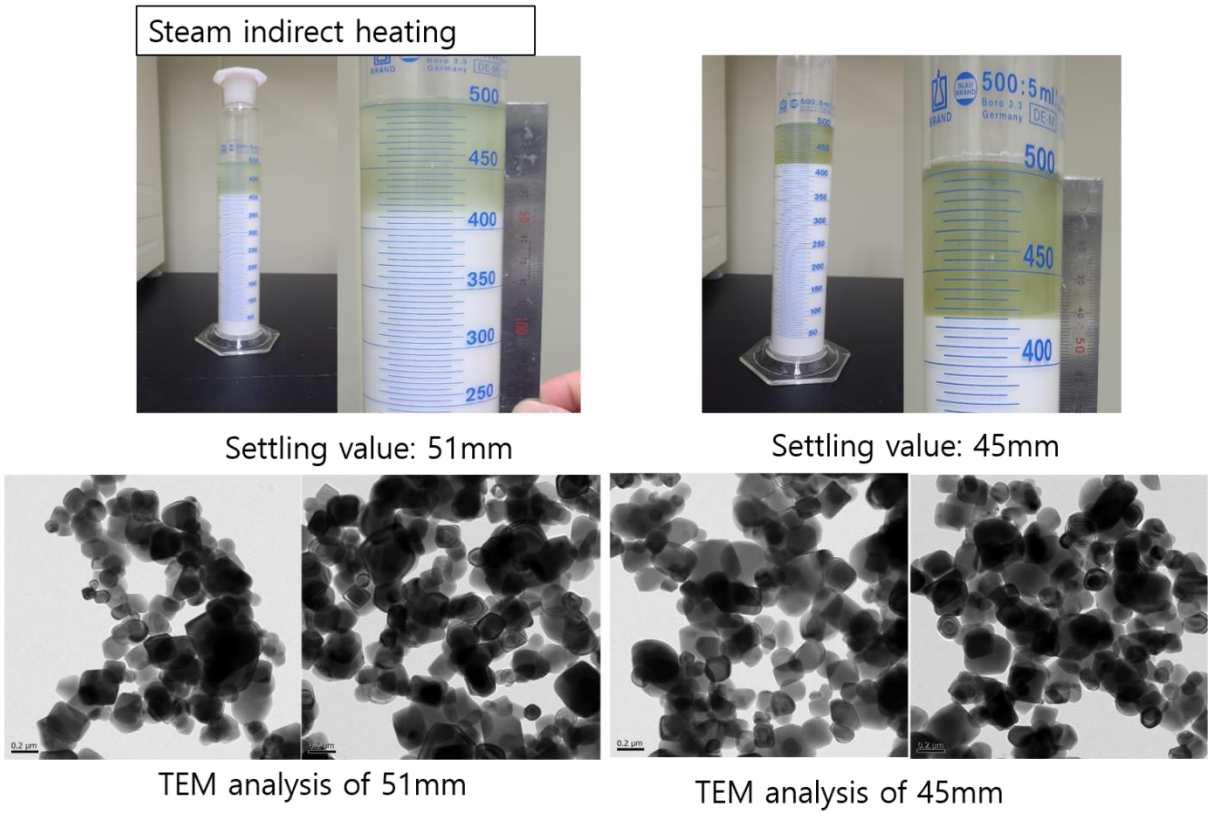
Steam indirect heating
500
450
400
350
300
250
Settling value: 51mm
500:5ml
Boro 3.3
Germany
500
450
400
Settling value: 45mm
TEM analysis of 51mm
TEM analysis of 45mm

Figure 6